Detailed Investigation of the Femtosecond Pump−Probe Spectroscopy of the Hydrated Electron

Kazushige Yokoyama, Carlos Silva, Dong Hee Son, Peter K. Walhout, and Paul F. Barbara*

Department of Chemistry, University of Minnesota, 207 Pleasant St. S. E., Minneapolis, Minnesota 55455

Received: April 9, 1998; In Final Form: June 26, 1998

We recently reported the first pump−probe measurements on the hydrated electron with sufficient time resolution (∼35 fs) to directly observe the initial processes in the solvation dynamics of this key prototype for condensed-phase dynamics [Silva, C.; Walhout, P. K.; Yokoyama, K.; Barbara, P. F. *Phys. Rev. Lett.* **1998**, *80*, 1086]. An unprecedented relaxation process for the hydrated electron was observed that occurs on the 35−80 fs time scale and exhibits a solvent isotope effect ($\tau(D_2O)/\tau(H_2O) \sim 1.4$). The new process was assigned to inertial/librational motion of the water surrounding the excess electron. The present paper reports a more extensive study of the ∼35 fs resolved dynamics of the hydrated electron in H_2O and D_2O at more probe wavelengths and as a function of pump-pulse intensity. The results are in agreement with the preliminary report and support the importance of librational water motion in the relaxation dynamics of the hydrated electron. New high excitation pulse intensity measurements reveal evidence of a high-intensity, two-photon channel involving ejection of the hydrated electron from its initial site to a different site in the solvent.

I. Introduction

Ultrafast studies on the solvated electron[1−19] in conjunction with quantum molecular dynamics simulations[20−32] are leading to important new insights on the molecular aspects of quantum dynamics in condensed phases. This research is also allowing for a rigorous evaluation of many of the most promising theoretical methods for condensed-phase dynamics. Much of the recent research on the hydrated electron has focused on transient pump−probe experiments on *equilibrated* excess electrons, involving excitation of the lowest energy electronic transitions of the hydrated electron ($\lambda_{max} = 720$ nm) and subsequent relaxation, which is observed to occur over a distribution of time scales ranging from 30 to ∼2000 fs.[1−3] The lowest energy electronic absorption band has been assigned to three overlapping transitions from the s-like ground state to the nondegenerate p-like excited states of the hydrated electron.[33−36] The s and p states are theoretically predicted to be localized at a particular site in the solution on the time scale of the s → p optical excitation and subsequent nonradiative relaxation. Pump−probe spectroscopy of the hydrated electron probes the s → p transitions and the p-to-conduction-band (CB) transition (of the photoexcited electron), as outlined in the upper panel of Figure 1.[3,20]

The nonradiative relaxation mechanism of the hydrated electron includes an *electronically nonadiabatic* component involving transitions between the nominal p-to-s states and among the three p sublevels. The nonradiative relaxation mechanism also includes *electronically adiabatic relaxation* processes within the s and p states, i.e., *solvation dynamics* of the hydrated electron. Nuclear motions of the water in the nearby surroundings of the excess electron are critically important in both the nonadiabatic and adiabatic components of the nonradiative relaxation. The relevant water motions are analogous to the types of solvent motions involved in the solvation dynamics associated with photoexcitation of polar molecular solutes in water.[37]

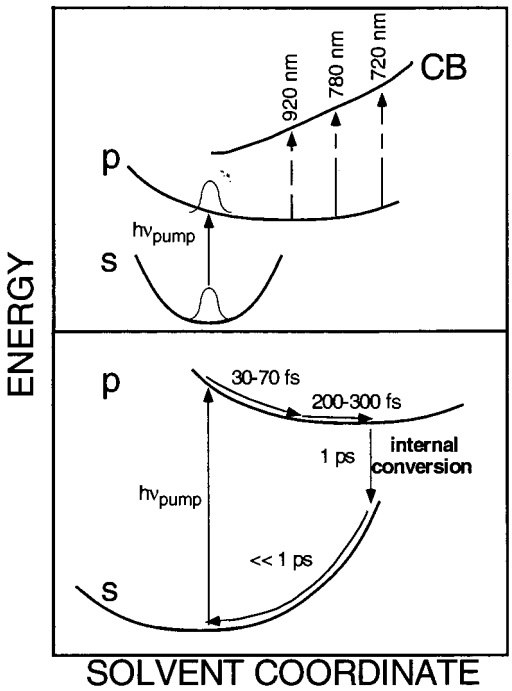

Figure 1. Schematic summary of the adiabatic solvation model of Schwartz and Rossky (see text). The complex spectral evolution following excitation (top panel) is ascribed to the evolution of the occupied p-state absorption spectrum and the evolution of the ground-state bleach. The lower panel shows the time scales for the adiabatic solvation versus the nonadiabatic (internal conversion) processes following photoexcitation of an equilibrated s-state electron.

Theory and simulation on the hydrated electron and polar molecular solutes quantify solvation dynamics in terms of the

* To whom correspondence should be addressed. E-mail barbara@chem.umn.edu.

S1089-5639(98)01809-X CCC: $15.00
Published on Web 08/07/1998

time correlation function of the s−p state energy gap, i.e., $S(t)$ or the related $M(t)$.[20,21,25,31,37,38]

$$S(t) = \frac{\langle U(t)\rangle - \langle U(\infty)\rangle}{\langle U(0)\rangle - \langle U(\infty)\rangle} \quad (1)$$

where $\langle U(t)\rangle$ is the nonequilibrium ensemble average of the time-dependent s−p energy gap. For water, $S(t)$ is predicted to exhibit relaxation components ranging from the tens of femtoseconds time scale to the picosecond time scale. Theory[39−43] and simulation[30,44−53] indicate that the polar solvation dynamics are dominated by solvent molecules in the first and second solvent shell. The most important molecular motions have been qualitatively classified as *inertial* librational solvent motion, inertial translational solvent motion, and diffusional (i.e., overdamped) rotational motion of the solvent. The inertial processes occur on the 30−50 fs time scale, involve so-called "free-streaming" motion of the solvent molecules, and possess an effective mass close to relevant free molecular motion, i.e., translation or rotation. The diffusional motion on the hundreds of femtoseconds and longer time scales are collective in character and have an effective mass which is much larger than a single water molecule.

For the hydrated electron, transient pump−probe features on the 35−80 fs time scale have been observed and assigned for the first time, based on the time scale of the dynamics and an observed ∼1.4 D_2O/H_2O isotope effect, to an inertial component of solvation dynamics involving substantial librational motion.[1] Transient fluorescence measurements on polar fluorescent probes in aqueous solution have also observed evidence of inertial solvation dynamics, but the limited time resolution in the latter type of measurements (100−110 fs instrument resolution) was insufficient to directly time-resolve this process.[54] This component of the solvent response has also been measured in other polar solvents in which more limited time resolution has been sufficient to observe such a response.[55−60] Additionally, Raman-induced Kerr effect studies of liquid water, in conjunction with depolarized Raman spectroscopy, have produced a model solvation time correlation function with a Gaussian component with a ∼25 fs width.[61,62] Interestingly, the observed isotope effect for the hydrated electron is larger than expected from some simulations on adiabatic solvation of the electron which predict that the inertial relaxation is predominantly translational in character.[22]

Due to insufficient information on the dependence of the solvated electron spectrum on the s−p energy gap, it has unfortunately not been possible to analyze the transient spectra to determine $S(t)$ for the hydrated electron. An additional complication in interpreting the hydrated electron spectrum results from ambiguity as to the assignment of the early time dynamics to adiabatic versus nonadiabatic relaxation. In particular, two alternative models have been proposed for assigning the experimentally observed pump−probe dynamics of the hydrated electron to specific molecular processes. One of these models (*adiabatic solvation*), which is summarized in Figure 1, ascribes the early time ≤300 fs spectral dynamics of the hydrated electron to adiabatic solvation in the lowest p state, observed via the p → CB (conduction band) transition.[20,21] According to this model, which is derived from nonadiabatic quantum molecular dynamics simulations, dynamics on slower time scales are a consequence of slower components of p state solvation and the p → s nonadiabatic transition. The dynamical processes are predicted to be reflected in the pump−probe spectroscopy via the "bleach" and recovery of the s → p absorption, the complex dynamical evolution of the p-state absorption, and the p → s stimulated emission, although this latter component does not significantly contribute to the spectroscopy in the visible to near-IR range. The alternative model, which we denote as *nonadiabatic relaxation*, assigns the initial relaxation components of the solvated electron (≤300 fs) to the p → s nonadiabatic transition, while the slower dynamics are ascribed to s-state adiabatic relaxation following the radiationless transition process.[3]

To address these issues and other aspects of the hydrated electron dynamics, new ∼35−60 fs resolved pump−probe measurements on the hydrated electron have been made and are reported in this paper. The measurements include a broad range of probe wavelengths and an extensive investigation of solvent deuterium isotope effects. Additionally, transient spectra have been studied as a function of the pump-pulse intensity. The new data have verified that previously reported dynamics[1] were due to single-photon s → p excitation. The high pump intensity results demonstrate that two-photon excitation of the hydrated electron leads to photoejection of the hydrated electron from its initial site. The new data also shed light on the relationship of *femtosecond pump−probe experiments* on the hydrated electron to the related but distinct *femtosecond photoionization experiments* on water which generates hydrated electrons.[6−11,13−17]

II. Experimental Section

Femtosecond laser pulses were generated with a home-built, argon-ion-pumped Ti:sapphire oscillator (15 fs, 800 nm, 3 nJ/pulse).[63] The femtosecond pulses were amplified at a 1 kHz repetition rate with a Nd:YLF-pumped, home-built multipass Ti:sapphire amplifier consisting of a three-mirror multipass ring configuration.[64] The amplified pulses (300 μJ/pulse) exhibited a 35 fs fwhm autocorrelation trace obtained with a 100 μm thick KDP crystal. Assuming a Gaussian pulse temporal profile, the 25 fs pulses were always within 5% of the transform limit.

Pump−probe experiments were performed at 1 kHz with a three-pulse sequence as described in previous studies.[1] The fourth harmonic of a Q-switched Nd:YLF laser (50 ± 10 μJ/pulse, 263.5 nm, 300 μm spot size (fwhm)) was used as a synthesis pulse to generate solvated electrons via one-photon electron photodetachment from aqueous $Fe(CN)_6^{4-}$. A portion of the output of the multipass amplifier was used as a pump pulse (which was variably delayed with respect to a probe pulse) to photoexcite the thermally equilibrated, ground-state electrons. The resulting spectral dynamics were monitored with the tunable probe pulse. The probe light for most of the measurements was selected from a single-filament white-light continuum generated by focusing 2 μJ laser pulses into a 3 mm thick sapphire crystal. A pair of LaKL21 prisms in a double-pass configuration were used for dispersion compensation of the continuum. A slit was placed after the first pass through the prism pair to select the desired portion of the continuum with sufficient bandwidth to support a 25−45 fs pulse. The separation of the two prisms was determined by minimizing the cross-correlation pulse width measured with a 100 μm KDP crystal via sum frequency mixing with the pump beam. For the measurements at 780, 800, and 820 nm a portion of the fundamental laser bandwidth (without the continuum generation optics and without prism compensation) was used for the probe. For the measurement probing at 600, 780, 800, 820, and 860 nm, we placed a 10 nm bandwidth interference filters in front of the detectors. An 850 nm long pass filter was used when the probe beam was centered at 920 nm, and no optical filter was used for the measurement probing at 720 nm. Typical

cross-correlation widths (fwhm) were 45 fs at 920 and 860 nm and 60 fs at 720 and 600 nm, and the autocorrelation of the pump pulse was 35 fs.

The sample consisted of a ∼300 μm jet produced by a stainless steel nozzle. The sample solution was circulated between a reservoir, the nozzle, and a heat exchanger (thermostated at 15 °C) by a Teflon/stainless steel gear pump. Aqueous solutions of 10 mM $K_4Fe(CN)_6$ (Aldrich) were prepared in HPLC grade H_2O or in D_2O (Cambridge Isotope Laboratories, 99.5% isotopic purity). To maintain a stable and flat sampling region within the jet, poly(ethylene oxide) (Polysciences, MW = 100 000) was added to the sample solution (0.5 wt %). It was confirmed that the observed femtosecond dynamics were not altered by the addition of poly(ethylene oxide).

The optical pump and probe beam spot sizes at the sample were 300 and 40 μm (fwhm), respectively. The energy of the pump pulse was typically 1−2 μJ ((2−4) × 10^{10} W/cm^2) except for the pump energy dependence study, where the energy of the pump pulse was varied from 30 nJ to 100 μJ by inserting calibrated neutral density filters. The intensity of the probe beam was maintained at ∼2 nJ for the entire measurement. The linearly polarized pump pulse was oriented at 54.7° with respect to the polarization of the probe pulse. The pump and probe beams crossed at a 4 ± 1° angle at the sample.

The detector hardware and associated electronics are similar to those described previously.[65] Some of the femtosecond measurements reported herein were recorded with a ∼300 fs resolution pump−probe spectrometer which has been previously described.[3] Briefly, a Nd:YLF-pumped (527 nm, 6 W, 2 kHz) Ti:sapphire regenerative amplifier was used. The available probe wavelength range (430−1150 nm) was obtained from frequency selection of a white-light continuum generated in quartz using a variable interference filter wheel. After amplification and recompression, the output consisted of 130 fs, 780 nm, 180 μJ pulses.

III. Results

A. Pump−Probe Measurements with One-Photon s → p Excitation. The most extensive set of data on the femtosecond pump−probe spectroscopy of the equilibrated hydrated electron are shown in Figures 2−4 and Table 1. These measurements were made with a pump pulse centered at 800 nm and a duration of 25 fs. The pump pulse was derived directly from the output of the multipass Ti:sapphire amplifier. The pump-pulse energy for the data in these figures was sufficiently low (<3 μJ) to ensure that the s → p excitation involved less than 10% depletion of the ground-state s population and that there was no significant component of absorption of a second photon from the excitation pulse. A more extensive discussion of pump pulse saturation and two-photon excitation is presented in a later section of this paper. The femtosecond data at most wavelengths (except at 780, 800, and 820 nm) were recorded with a variable wavelength probe pulse generated from a white-light continuum. The dispersion compensation prism system for the continuum and the associated optics restricted the bandwidth before the sample to approximately 40 nm centered around the chosen probe wavelength. In some cases an additional interference filter was used before the detector to reject the scattered pump light and any spurious emission associated with the UV synthesis pulse of the hydrated electron. All transients were corrected for a small artifactual signal centered around zero delay caused by pump-induced phase modulation of the probe. These artifacts were typically less than 1% of the total signal and in the largest cases were approximately 5%.

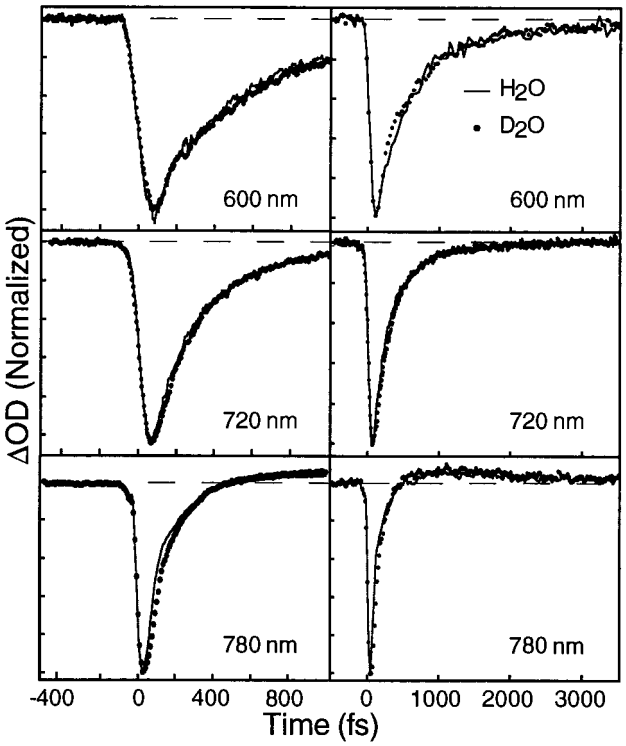

Figure 2. Transient ΔOD (change in optical density) signal as a function of pump−probe delay for the solvated electron in 10 mM $K_4Fe(CN)_6$ in H_2O (solid lines) and D_2O (data points) solutions, probing at 600, 720, and 780 nm. The 800 nm, 25 fs, 1−2 μJ pump pulse was linearly polarized at 54.7° with respect to the linearly polarized probe pulse. The plotted ΔOD signals are normalized for comparison of the data. The maximum ΔOD is ≤10 mOD at 720 nm. Each transient is fit to a model function consisting of a Gaussian plus two exponential components convoluted with the instrument response function (fits not shown; see Table 1 for details).

The pump−probe data near the center of the absorption band and at shorter wavelengths (Figure 2) are dominated by an initial bleach at early delays followed by a bleach recovery on a distribution of time scales. The fastest of the time scales in this region of the spectrum is in the range 50−80 fs and corresponds to as much as 50% of the recovery at a probe wavelength of 780 nm. The initial fast component of the decay is better fit in this wavelength range by a Gaussian decay component rather than an exponential. As a result, we have routinely fit the 35 fs resolved pump−probe data of the hydrated electron with a model function that includes one Gaussian decay component and two additional exponential components, as shown in the title of Table 1. The use of the Gaussian decay component for the initial decay is further suggested by simulations on the hydrated electron which indicate that the initial decay of the energy gap correlation function $S(t)$ is approximately Gaussian.[20,28,30,49] As mentioned in our recent preliminary report on these measurements, the Gaussian component corresponds to a significant fraction of the total decay, and this decay component had been missed in earlier experiments with lower time resolution, which were only able to resolve the decay component that occurs on the 300 fs and longer time scale. Thus, the average decay times, $\langle\tau\rangle$, reported in this paper are significantly shorter than those previously reported with 300 fs resolution[3] since the new measurements include the initial femtosecond decay component represented by a Gaussian.

At longer probe wavelengths (Figure 3) the initial bleach of the hydrated electron is clearly observed to recover to a positive (absorption) signal which decays on a slower time scale. These

TABLE 1: Parameters from Fits of the Model Function, $\Delta OD = A_G \exp(-t^2/2\tau_G^2) + A_1 \exp(-t/\tau_1) + A_2 \exp(-t/\tau_2)$, to the Pump−Probe Signals (Change in Optical Density) for Excess Electrons in H_2O and in D_2O at 288 ± 2 K[a]

solvent	λ (nm)	τ_G (fs)	A_G	τ_1 (fs)	A_1	τ_2 (fs)	A_2	$\langle\tau\rangle$ (fs)[b]
H_2O	600	59 ± 23	−0.26 ± 0.08	497 ± 98	−0.66 ± 0.07	1952 ± 107	−0.08 ± 0.06	376 ± 87
	720	79 ± 5	−0.26 ± 0.03	263 ± 9	−0.65 ± 0.05	630 ± 43	−0.09 ± 0.02	215 ± 5
	780	51 ± 6	−0.47 ± 0.04	220 ± 12	−0.47 ± 0.03	2140 ± 433	0.06 ± 0.01	142 ± 11
	800	69 ± 9	−0.30 ± 0.08	194 ± 24	−0.60 ± 0.08	2049 ± 332	0.10 ± 0.01	156 ± 12
	820	58 ± 7	−0.32 ± 0.06	173 ± 16	−0.56 ± 0.06	1807 ± 76	0.11 ± 0.01	154 ± 13
	860	48 ± 17	−0.35 ± 0.12	91 ± 11	−0.42 ± 0.14	1120 ± 183	0.22 ± 0.01	154 ± 13
	920	32 ± 8	−0.28 ± 0.1	99 ± 21	−0.39 ± 0.10	814 ± 116	0.33 ± 0.02	73 ± 8
D_2O	600	57 ± 25	−0.27 ± 0.15	53 ± 62	−0.66 ± 0.15	2000[c]	−0.07 ± 0.04	446 ± 49
	720	120 ± 13	−0.19 ± 0.06	271 ± 27	−0.73 ± 0.08	905 ± 200	−0.08 ± 0.07	244 ± 16
	780	75 ± 10	−0.38 ± 0.05	222 ± 23	−0.54 ± 0.06	2007 ± 678	0.08 ± 0.01	169 ± 13
	800	102 ± 6	−0.29 ± 0.08	210 ± 27	−0.59 ± 0.08	1705 ± 319	0.12 ± 0.01	181 ± 12
	820	97 ± 9	−0.33 ± 0.08	185 ± 23	−0.52 ± 0.09	1631 ± 234	0.15 ± 0.02	159 ± 10
	860	88 ± 5	−0.39 ± 0.16	104 ± 16	−0.32 ± 0.17	953 ± 125	0.28 ± 0.01	108 ± 10
	920	81 ±17	−0.30 ± 0.19	100[c]	−0.35 ± 0.21	832 ± 134	0.33 ± 0.01	99 ± 4

[a] The sum of individual amplitudes was normalized to unity. The errors are one standard deviation from the mean of multiple measurements (typically >20). [b] The average time constant is defined by $\langle\tau\rangle = [(\pi/2)^{1/2}A_G\tau_G + A_1\tau_1]/(A_G + A_1)$. [c] The time constant at these wavelengths was held constant at the indicated value. The quality of the fits did not change significantly when this parameter was allowed to float.

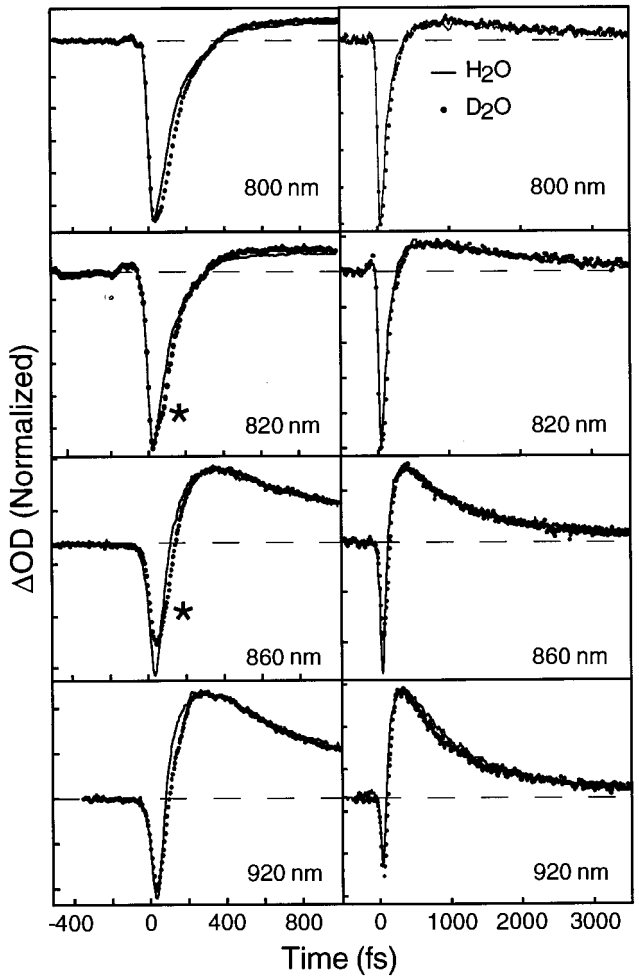

Figure 3. Similar to Figure 2, but probing at 800, 820, 860, and 920 nm.

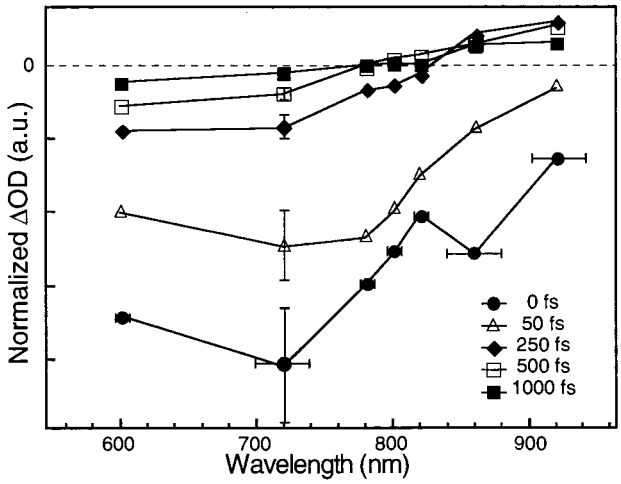

Figure 4. Transient ΔOD (change in optical density) as a function of wavelength and after various pump−probe delays for the hydrated electron in 10 mM $K_4Fe(CN)_6$ solutions. The ΔOD signals are comprised of various measurements at various powers within the linear pump absorption regime, normalized by the pump power. Typical ordinate error bars for all delays and all wavelengths are displayed for the data at 720 nm. The spectral bandwidth reaching the detectors is indicated by the error bars in the abscissa for the data at zero delay. (See text for a detailed description of the frequency filters that were used.)

data are consistent with both the previous 300 fs measurements which are unable to observe the initial fast decay component and with the recently reported but less extensive measurements with 35 fs resolution.[1] Figure 4 presents the transient data in the form of a ΔOD spectrum at different probe delay times. The data were constructed from the best fits of the model function in Table 1 to the individual wavelengths for the pump−probe spectroscopy of the hydrated electron. The data clearly show that the initial fast Gaussian decay component corresponds to the partial recovery of the bleach signal at all wavelengths probed in these experiments. Additionally, the bleach signal at all wavelengths further recovers on the hundreds of femtoseconds time scale. The spectral characteristics shown in Figure 4 can be equally well explained by either the *adiabatic solvation model*[20,21] or the *nonadiabatic relaxation model*[3] (see Introduction). In the former case the dramatic spectral changes seen in Figure 4 on time scales <250 fs are attributed to overlapping bleach signals for the s-state electron and the excited-state absorption spectrum that is evolving as the s−p gap decreases rapidly during the p-state lifetime due to solvation. On the other hand, in the nonadiabatic relaxation model the rapid decay (i.e., 50 fs, 300 fs, or both) is due to p → s internal conversion, and the slower dynamics are associated with relaxation in the ground state. It is unclear which of these models correctly accounts for the observed dynamics.

It is important to note that there are additional features in the pump−probe data that are not well modeled by the simple dynamical function in Table 1. This is demonstrated in Figure 3. The initial positive-going signal before the bleach of the hydrated electron signal (800 and 820 nm) has been attributed

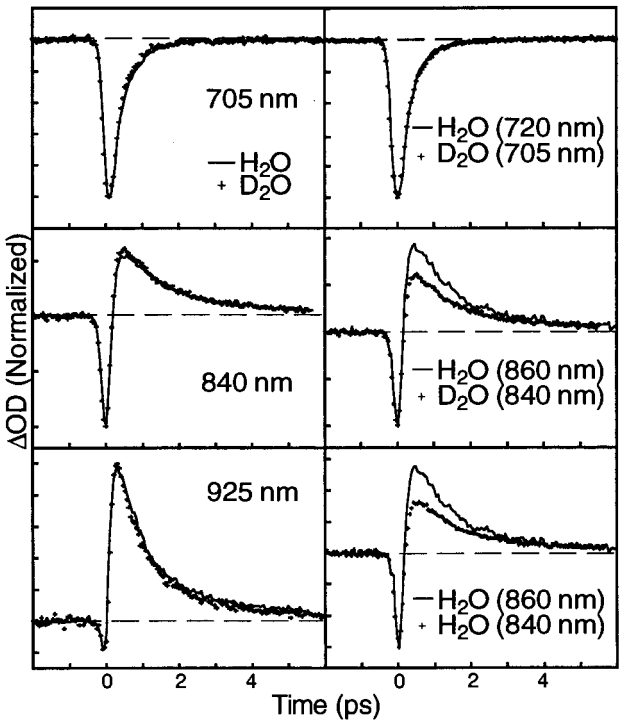

Figure 5. A comparison of transient ΔOD (change in optical density) signal of the solvated electron in 1 mM $K_4Fe(CN)_6$ in H_2O (solid lines) and D_2O (data points) solutions with 300 fs time resolution, obtained in a flow cell with a 1 mm path length. The probe wavelengths are indicated in each panel.

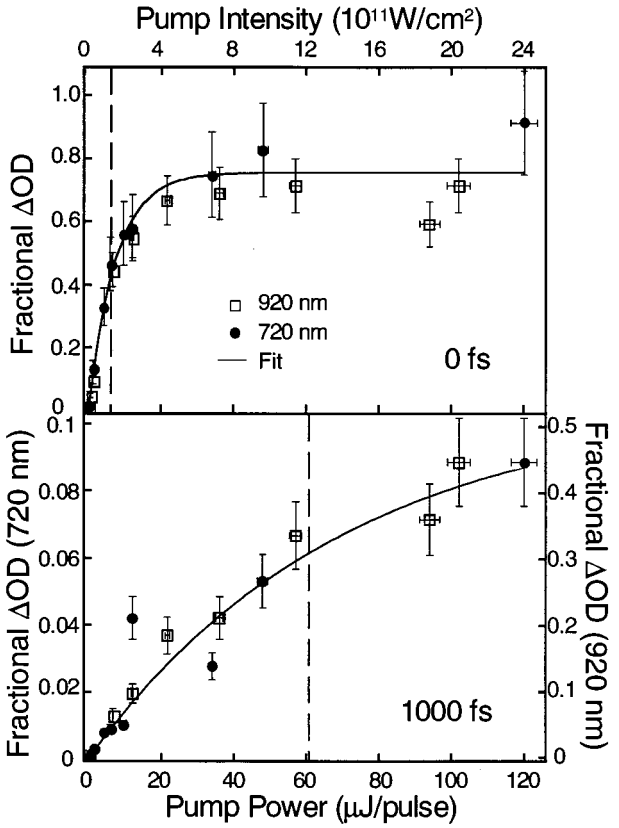

Figure 6. Top panel: initial ΔOD (change in optical density) as a function of pump-pulse intensity, measured at 720 and 920 nm. The initial ΔOD was obtained from the fit to a multiexponential function and was normalized by the initial absorption of the hydrated electron created by the UV synthesis pulse. The solid line represents a fit to the expression $A\{1 - \exp(-I/I_S)\}$ where I_S is the saturation intensity $((1.5 \pm 0.3) \times 10^{11}$ W/cm^2). Bottom panel: fractional ΔOD as a function of pump intensity 1 ps after excitation, probing at 720 nm (left axis) and 920 nm (right axis). The solid line is a fit to the same function as in the top panel, with $I_S = (1.2 \pm 0.3) \times 10^{12}$ W/cm^2. The broken lines in each panel indicate the saturation intensity.

to a coherent interaction of the pump and probe signal by Wiersma and co-workers.[66] Additionally, the so-called "bump" in the signal (marked by the asterisk at 820 and 860 nm) is also not well described by the model decay function and apparently reflects some type of wave packet dynamics.[66] We return to the question of wave packet dynamics of the hydrated electron in the Discussion section.

The data represented in the figures and Table 1 show a significant D_2O/H_2O effect on the dynamics of the hydrated electron. This effect is primarily associated with the initial decay component and is nearly undetectable at times longer than approximately 200 fs. At each of the probe wavelengths a D_2O/H_2O effect is observed. However, it is most dramatic at the redder wavelengths. The D_2O/H_2O deuterium solvent isotope effect on the lifetime of this component is 1.6 ± 0.5. We have argued previously that this isotope effect is indicative of substantial librational character in the initial decay.[1] This will be discussed extensively below.

One important complication in interpreting the D_2O/H_2O isotope effect is the possibility that there may be an isotope effect on the energies of the s and p states, resulting in spectral shifts in the H_2O versus the D_2O data. Thus, it may be difficult to directly compare the apparent dynamics in the two solvents since the spectra may be significantly shifted. There is some evidence to support the importance of this complication since the s → p absorption maximum of the hydrated electron was reported to have a nearly 15 nm blue shift in D_2O versus H_2O.[67]

To explore this possibility further, we studied the transient spectroscopy of the hydrated electron in H_2O and D_2O with a high signal-to-noise ratio at various probe wavelengths as summarized in Figure 5. These data were acquired with our earlier femtosecond spectrometer that had a ∼300 fs time resolution. The data in Figure 5 clearly show that the pump−probe dynamics in H_2O and D_2O are identical at the same probe wavelength in this long time range. If one attempts to make comparisons between dynamics at different probe wavelengths in order to compensate for the previously reported 15 nm isotope shift in the spectrum maximum, the data show dramatic differences that appear to result primarily from the spectral dependence of the kinetics rather than anything due to an isotope shift. Thus, the comparison of the H_2O data at 860 nm to the D_2O data at 840 nm produces the same variation as simply comparing the H_2O data alone at these different probe wavelengths. The main conclusion, therefore, is that static spectral shifts due to isotopic substitution is not a complication in interpreting the isotope effects on the pump−probe dynamics of the hydrated electron.

B. Pump Intensity Dependence. The transient data shown in Figures 2−4 have been recorded with pump-pulse energies that induce only a small (<10%) depletion of the ground s-state population. This is demonstrated in the upper panel of Figure 6 which plots the relative optical density of the initial bleach ($t \approx 0$) in transients at 920 and 720 nm as a function of the pump-pulse energy. The data are normalized by the optical density of the s → p absorption in the absence of the pump pulse and corresponds to the fraction of the initial s → p absorption signal that is bleached ("bleach"). The conclusion that in this pump intensity range the data are due to one-photon excitation of the s → p transition is further supported by the data in Figure 7. These data show that the observed transients in the low-

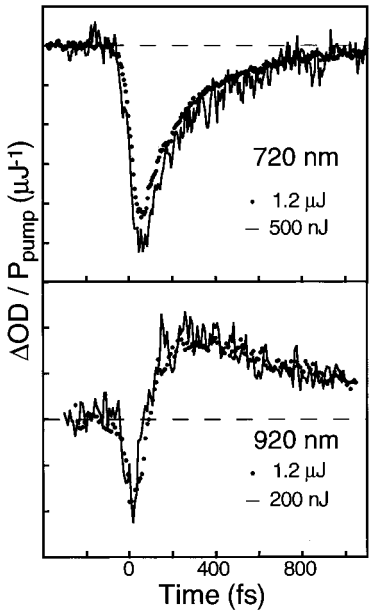

Figure 7. Transient ΔOD (change in optical density) signal of the hydrated electron pumping with either 1.2 or ~0.5 μJ pulses and probing at 720 or 920 nm. The data are normalized by the pump-pulse energy and are superimposed to show the linearity of the signal.

intensity regime, when linearly corrected for variation of pump intensity, are identical within the experimental error except for the additional noise observed in the lower pump intensity data.

The initial fractional bleach data in the upper panel of Figure 6 are qualitatively consistent with a simple two-state kinetic model, i.e., model 1 in Figure 8. In terms of this model the observed saturation intensity, $I_S = (1.5 \pm 0.3) \times 10^{11}$ W/cm^2 (derived from a fit to a simple photodepletion expression), is consistent with the known s → p cross section at the pump wavelength. The model is only consistent with fractional bleach data for p → s lifetimes >300 fs. For substantially shorter lifetimes, the predicted I_S is much larger that observed experimentally. Thus, a simple two-state model interpretation of the data indicates that for measurements with pump intensities ≤5 μJ less than 10% of the s electrons are excited. This is the regime that corresponds to the data in Table 1 and Figures 2−4. Furthermore, the analysis suggests that the s-state recovery time is ≥300 fs, which is evidence *against* the nonadiabatic relaxation model (at least in the case of a p-state lifetime of ~50 fs).

It should be emphasized that model 1 is certainly too simple to describe the complex dynamics of the hydrated electron, since it lacks dynamical processes that can account for the multiple time scales that are experimentally observed. Model 1 also fails to predict the dynamical effects that are observed in the pump−probe data for high pump energies. In particular, when the pump intensity is increased significantly, especially above 20 μJ (4×10^{11} W/cm^2), the data exhibit a substantial dependence on the pump pulse energy. This is shown in Figure 9. The strong variation in the kinetics in Figure 9 are not the simple consequence of saturation of the s → p transition, even in the regime where rapid ground-state recovery is followed by further s → p absorption. This has been demonstrated by carefully considering the effect of the saturation on the s → p transition using a kinetic model that convolutes the pump intensity profile in space and time with model 2 in Figure 8. Model 2 includes a rapid p → s relaxation followed by slower adiabatic relaxation in s. Simulations with model 2, shown in the top panel of Figure 10, fail to predict the change in the observed kinetics at high pump power (top panel, Figure 9).

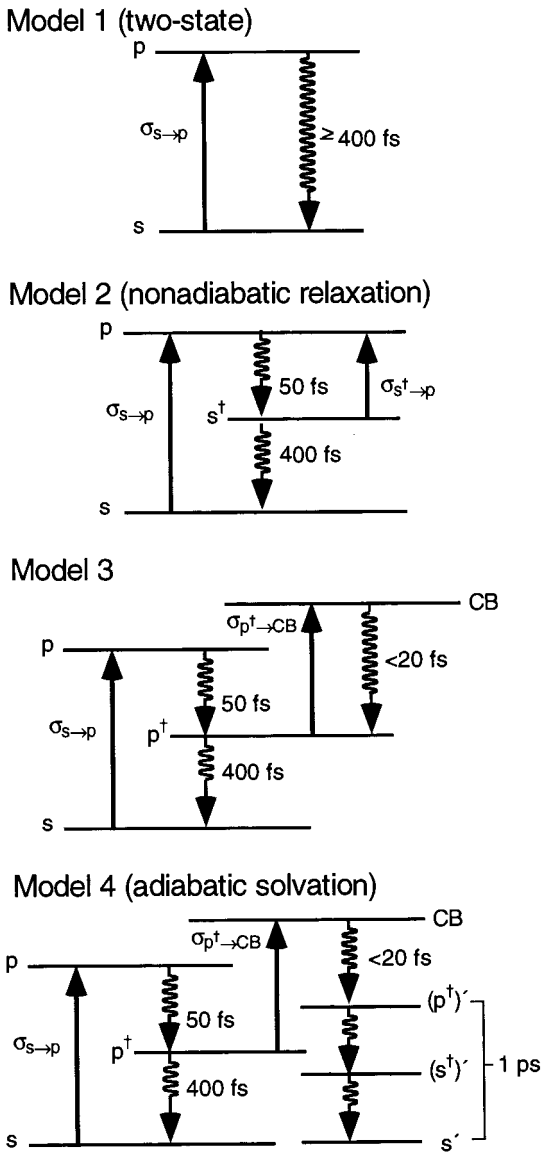

Figure 8. Schematic diagrams of kinetic models used to simulate the dynamics (Figure 10). Here σ is the absorption cross section. The superscript cross symbol (†) denotes a nonequilibrium s or p state, while the prime denotes an electron that has retrapped at a site that is different from the original one.

Another model that cannot account for the data is model 3 in Figure 8 which is based on the assumption that excited-state absorption (p → CB) simply results in rapid repopulation of p. This model also fails to predict the slow dynamics that are observed at high pump power.

The experimentally observed dynamics can, however, be accounted for by model 4 in Figure 8. In this model, sequential two-photon absorption (i.e., s → p and p† → CB) produces CB electrons which are assumed to rapidly migrate to a new site in the solvent (which is indicated by a prime). Furthermore, it is assumed that relaxation at the new site is slower than relaxation at the original site since the solvent configuration in the new site is not "preequilibrated". (The relaxation at the new site is arbitrarily assumed to occur on the ~1 ps time scale in model 4.) The relaxation at the new site may involve a combination of s′ and p′ state adiabatic solvation as well as p′ → s′ nonadiabatic relaxation. Predictions from model 4 (bottom panel in Figure 10) are qualitatively consistent with experiment (Figure 9).

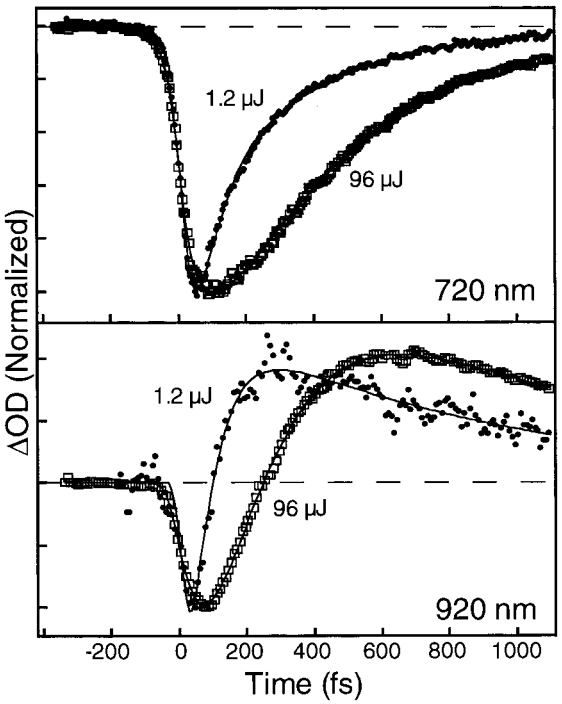

Figure 9. Comparison of the transient ΔOD (change in optical density) signals of the hydrated electron pumping with either 1.2 or 96 μJ pulses, and probing at either 720 or 920 nm. The data are normalized to the same maximum negative signal (*not* by the pump energy as in Figure 7) and are superimposed to demonstrate the pump-pulse energy dependence on the dynamics. The solid lines are the results from the fit to a Gaussian-plus-two-exponential functions convoluted with the instrument response function.

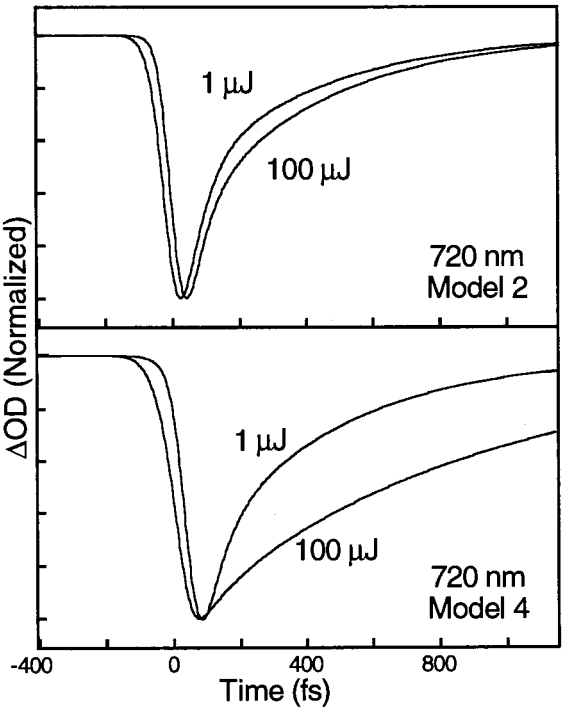

Figure 10. Simulated ΔOD (change in optical density) signal probing at 720 nm with the use of model 2 (top panel) and with the use of model 4 (bottom panel). Each panel shows two curves derived from the simulation using a pump energy of 1 and 100 μJ.

Further evidence that the high pump intensity dynamics are due to a sequential two-photon process is found in the pump intensity dependence after a 1 ps pump−probe delay (bottom panel, Figure 6). The data in this figure also fit well to a simple photodepletion expression, but the saturation intensity is $I_S = (1.2 \pm 0.3) \times 10^{12}$ W/cm^2, nearly an order of magnitude larger than that at zero delay. This is interpreted as saturation of the p → CB transition.

IV. Discussion

The pump power dependence of the pump−probe spectroscopy of the equilibrated hydrated electron strongly suggests that the dynamics at low pump power are primarily due to single-photon excitation of s-like electrons to the Franck−Condon geometry of p-like electrons. Theoretical simulations for the hydrated electron indicate that the p sublevel relaxation is considerably faster than other types of dynamics.[20] Consequently, the primary processes that are expected to contribute to the observed dynamics are p-state adiabatic solvation, s-state adiabatic solvation, and p → s nonadiabatic relaxation. As mentioned previously, the exact assignment of these processes to the particular relaxation time scales summarized in Table 1 is somewhat ambiguous. In particular, whether the ∼50 fs major decay component in the dynamics is p-state adiabatic solvation or p → s nonadiabatic relaxation is still somewhat in doubt. Nevertheless, the analysis of the saturation dependence of the initial bleach in the pump−probe data tends to disfavor the interpretation of this component as nonadiabatic relaxation.

According to the p-state adiabatic solvation model, both s → p and p → CB absorptions are significant at all of the probe wavelengths reported in this paper. In particular, the transient data probing at 920 nm is assigned to an initial s → p bleach followed by a delayed absorption of the p state (p → CB) as it blue-shifts into the probe wavelength region. The ∼1 ps decay time at 920 nm is assigned to the actual p → s nonadiabatic transition. This model predicts very different behavior at 720 nm. The s → p bleach is almost exactly canceled by the absorption of the equilibrated p → CB absorption band, giving rise to a pseudoisosbestic point in this spectral region.[5,10,11] Thus, at this wavelength the dynamics primarily reflect the early evolution of the p-state absorption due to adiabatic solvation. Furthermore, at shorter wavelengths, for example, 600 nm, the s → p bleach is only partially canceled by the p-state adiabatic solvation and p → s nonadiabatic transition. This model implies that the adiabatic solvation of the p state can be directly monitored at all wavelengths that are summarized in Table 1. Nevertheless, since the actual Franck−Condon factors of the p → s and p → CB absorption are not known and, additionally, the evolving electronic matrix element for the absorption is not well understood, it is not actually possible to directly determine an evolving energy gap for p → s during the adiabatic solvation process. Consequently, while the data clearly show spectral evolution on the ∼50 fs time scale and on the 200−300 fs time scale, and this evolution is probably due to adiabatic p-state solvation, it is not possible to definitively associate the time scale of these dynamics with the relaxation processes in the energy gap correlation function.

It is interesting to compare the observed femtosecond pump−probe data to recent quantum molecular dynamics (MD) simulations of this type of experiment. Unfortunately, the simulations are restricted to a time resolution of 300 fs, which was built into the simulations to compare with previous, lower time resolution experiments.[21,22,25,26] New simulations will be required to make a direct comparison to the early time pump−probe dynamics. The published simulation results include the time-dependent s−p quantum energy gap of the hydrated electron, which was analyzed to determine the nonequilibrium solvent response function, $S(t)$. Since this function measures the adiabatic solvation of the p state, one would expect at least a

rough correlation of this function with the observed evolution of the transient spectrum. The simulated $S(t)$ due to Schwartz and Rossky has been well fit by a model decay function involving a Gaussian decay (~25 fs, 38% amplitude) due to inertial motion of the H_2O molecules and an additional exponential decay (~250 fs diffusive solvation).[20] These time scales are also in agreement with adiabatic MD simulations of excess electrons in water clusters by Barnett et al.[30] and with other related simulations on the hydrated electron[28,49] and other charged species undergoing solvation dynamics in water.[44−48] Qualitatively, our results are consistent with the simulations in both the observation of a large-amplitude Gaussian component of dynamics on the tens of femtoseconds time scale and the observation of a slower component on the ~300 fs time scale. However, the fast dynamical component that we assign to inertial relaxation is significantly slower than that predicted in the MD calculations. Whether this discrepancy is a consequence of the failure of the models or whether it has something to do with the failure of the absorption transients to track $S(t)$ is unknown. Future simulations will hopefully address this issue in more detail.

As mentioned in our preliminary report of the ~35 fs measurements of the pump−probe spectroscopy of the hydrated electron, our spectrometer has sufficient time resolution to rule out a spectral dynamic component with a 25 fs time scale.[1] Thus, the failure to observe evolution on the 25 fs time scale is not a consequence of experimental limitations. Furthermore, the experimental results show a clearly resolved D_2O/H_2O isotope effect of 1.51 ± 0.29 (at 800 nm). This isotope effect is larger than predicted by the MD simulations of adiabatic solvation for the hydrated electron by Schwartz and Rossky.[20] However, the adiabatic MD simulation by Barnett et al. does report an isotope effect of this magnitude.[30] The discrepancy between our observed isotope effect and that predicted by simulations is a critical issue in the comparison of theory and experiment of the solvation dynamics of excess electrons. The presence of the isotope effect strongly suggests that the initial solvation dynamics are dominated by librational motion of the water molecules. In contrast, the MD simulations by Schwartz and Rossky indicate a broader distributions of molecular motions in the initial solvation component including translational solvent modes. Thus, the experiments tend to suggest that the early time dynamics of the electron are qualitatively different at the molecular level than simulations suggest. Considerably more work will be necessary to firmly establish this apparent discrepancy between theory and experiment. One possible explanation for the discrepancy is that the observed ~50 fs component may have significant nonadiabatic character associated with this process. For example, it may be that this dynamic component is in fact due to p → s nonadiabatic transition, rather than adiabatic solvation, despite the evidence supporting the adiabatic solvation model. Alternatively, the initial dynamics may be partly due to relaxation among the p sublevels.

Figure 5 demonstrates that there is no significant isotope effect on the >300 fs dynamics of the hydrated electron. Within the excited-state adiabatic solvation model (Figure 1) the picosecond kinetic components of the data are interpreted as a consequence of the p → s nonadiabatic transition. The absence of an observed isotope effect for the p → s decay rate is consistent with recent nonadiabatic MD simulations by Rossky and co-workers, which predict that although the nonadiabatic coupling between the s and p states in D_2O is a factor of ~2 smaller than in H_2O due to slower nuclear velocities,[22] the decay of quantum coherence after nonadiabatic coupling takes ~50% longer in D_2O.[23] The smaller nonadiabatic coupling, therefore, acts coherently for a longer period of time in D_2O. The two effects cancel out, and only a small net isotope effect on the radiationless transition time constant survives. Other nonadiabatic MD simulations by Neria and Nitzan predict a factor of ~4 isotope effect on the p → s transition time,[31] which is clearly inconsistent with the results presented in this paper. A significant isotope effect is also predicted by a recent statistical theory for the hydrated electron by Bratos, Borgis, and co-workers.[26] This isotope effect is predicted to be the largest at the wings of the absorption band, and small near the pump frequency, since the spectral evolution near the pump frequency is predicted to be due to a "coherent spike" superimposed on a "thermic band". The latter is dependent on the nonadiabatic rate constant. Our results show that the largest isotope effect occurs at the red edge of the absorption band (920 nm), and the smallest at the blue edge (600 nm), with a ~1.4 isotope effect near the pump frequency, in apparent disagreement with the predictions from this theory. It is also interesting to compare the results to a simple hydrodynamic theory by Rips, which predicts a ~5% isotope effect on the radiationless transition time, in agreement with the data reported in this paper.[68]

Another interesting aspect of the experimental data is the apparent manifestations of coherent nuclear wave packet dynamics as indicated by the apparent "bump" in the data marked by the asterisk in Figure 3. Coherent wave packet dynamics were recently identified by Wiersma and co-workers in the pump−probe spectroscopy of the hydrated electron using ~15 fs pulses.[66] The features in Figure 3 are apparently not the consequence of such nonlinear processes as pump-induced cross-phase modulation of the probe and other high-order processes. Rather, the reproducibility of the measurements and the isotope effect on the magnitude and peak time of the feature in the transients suggests that the feature is due to some kind of coherent excitation of the vibrational motion caused by the s → p excitation.

As mentioned earlier, a multiphoton channel becomes important in the pump−probe experiments on excess electrons at high excitation intensities. This two-photon channel is closely analogous to the standard two-pulse photoinjection experiment and to charge-transfer-to-solvent (CTTS) transitions,[69−77] as schematically represented in Figure 11. Injected electrons that are produced by multiphoton ionization (either directly to the CB or through an excited state of water depending on the photon energy; see ref 9) must seek an appropriate trap such as site 1 in Figure 11A and localize either in a p state or in the s state. In the high-intensity pump−probe experiment, two-photon excitation of the equilibrated hydrated electron produces a CB electron, where it may seek a new site in which to retrap (site 2). The formation of fully equilibrated s′ electrons involves the same relaxation processes as those manifested in the injection experiments. This statement is supported by the role played by the slow kinetic components of the data. The time scales of the slow components in the high-intensity regime are similar to those observed in photoinjection experiments, which play a major role in the data. On the other hand, the slow components play a lesser role in the one-photon pump−probe data. Direct comparison of the photoinjection and photoexcitation experiments for the hydrated electron is rather dubious due to the presence of unsubtractable artifacts in experiments which use a very high-intensity photoionization pulse[16,17] and also due to the limited signal-to-noise ratio and time resolution in the two-pulse data[11] that has been reported in the literature. However, similar high excitation intensity effects have been observed by us for the solvated electron in alcohols,[5] where the time scales for fast and slow relaxation kinetic components are better

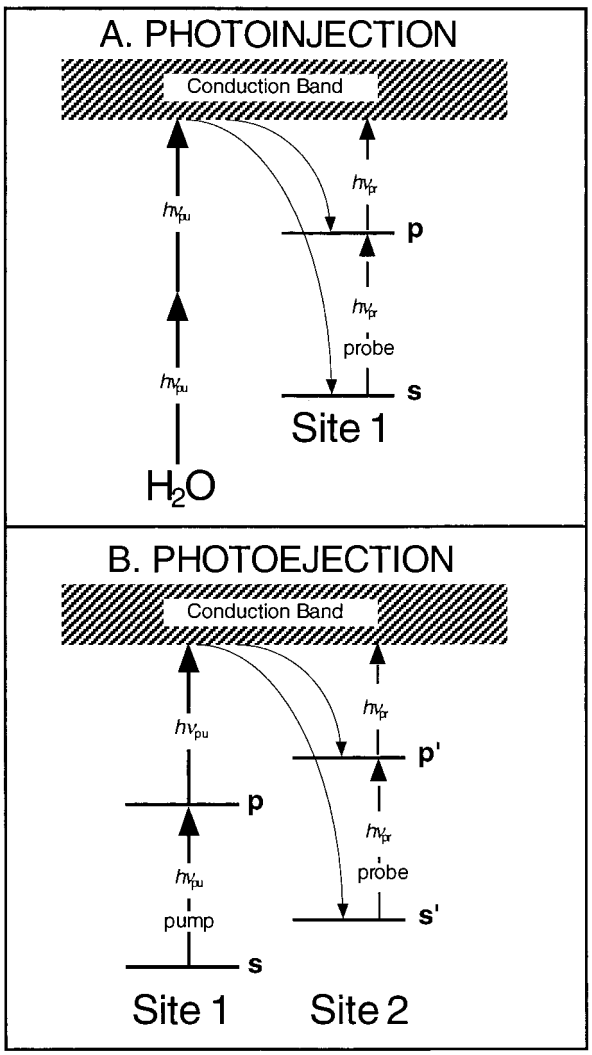

Figure 11. Schematic illustration comparing the electron photoinjection experiment (A) with the photoejection and retrapping experiment (B). In the photoinjection experiment an injected electron localizes in an s or p state. In the pump−probe experiment one-photon excitation of an s-state electron in site 1 produces a (localized) p-state electron in site 1. Two-photon excitation produces a CB electron, which may localize in a different solvent site (site 2).

separated. In that case, the correspondence of the slow time scales in the two-pulse and the (high excitation intensity) three-pulse experiments is clear. Moreover, a detailed excitation intensity dependence on a photoinduced proton-transfer reaction between the alcohol solvent molecules and the solvated electron suggested that the reaction is due to a two-photon process.

It is interesting to compare the concept of the CB electron produced by two-photon excitation of equilibrated hydrated electrons to a related concept in radiation chemistry, the "dry" electron. Upon radiolysis of water a transient species with energy well above the thermal energy, the dry electron, is formed.[78] This leads one to compare the CB electrons prepared in our pump−probe experiments via two-photon excitation with the highly reactive "dry" electrons discussed in the radiation chemistry literature. This suggestion opens the door for future studies of CB electron structure and dynamics, since climbing up the energy ladder from the ground state represents a new way of producing dry electrons.

V. Summary and Conclusions

We have performed detailed femtosecond pump−probe measurements on the equilibrated hydrated electron over a broad probe wavelength range and with sufficient time resolution to observe inertial solvation dynamics. The data are consistent both with earlier measurements with more limited time resolution[3] and with our recent preliminary report on the hydrated electron.[1] The spectral evolution following s → p photoexcitation is complex and reflects the involvement of transient solvation effects in the p → s radiationless decay dynamics of the solvated electron. Rapid spectral evolution (on a 30−80 fs time scale) is observed, followed by evolution on slower time scales (∼200−300 fs, ∼1 ps). Pump-pulse intensity dependence studies reveal that the observed complex spectral evolution is due to a one-photon excitation regime at low pump intensity and a two-photon excitation regime at high pump intensities. The one-photon regime is assigned to excitation and subsequent relaxation between s- and p-like states that are localized in the same solvent "site". In contrast, the two-photon regime is assigned to sequential two-photon excitation of the electron producing conduction band electrons which ultimately are trapped at new solvent sites.

The comparison with nonadiabatic quantum molecular dynamics simulations supports the general validity of the theoretical treatments and leads to new insights on the molecular details of the solvation relaxation processes of the hydrated electron. While more work needs to be done in both experimental and theoretical fronts to assign the observed dynamics features to adiabatic solvation or nonadiabatic relaxation processes, analysis of the power dependence data supports the validity of the excited-state adiabatic solvation model. Furthermore, the data are in agreement with the MD simulations that predict small isotope effects on the p-state lifetime. These results provide an important step toward an understanding of the hydrated electron photoinjection and pump−probe experiments.

Acknowledgment. This research was supported with a grant from the DOE-BES.

References and Notes

(1) Silva, C.; Walhout, P. K.; Yokoyama, K.; Barbara, P. F. *Phys. Rev. Lett.* **1998**, *80*, 1086.
(2) Alfano, J. C.; Walhout, P. K.; Kimura, Y.; Barbara, P. F. *J. Chem. Phys.* **1993**, *98*, 5996.
(3) Kimura, Y.; Alfano, J. C.; Walhout, P. K.; Barbara, P. F. *J. Phys. Chem.* **1994**, *98*, 3450.
(4) Walhout, P. K.; Alfano, J. C.; Kimura, Y.; Silva, C.; Reid, P. J.; Barbara, P. F. *Chem. Phys. Lett.* **1995**, *232*, 135.
(5) Silva, C.; Walhout, P. K.; Reid, P. J.; Barbara, P. F. *J. Phys. Chem. A* **1998**, *102*, 5701.
(6) Sander, M.; Brummund, U.; Luther, K.; Troe, J. *Ber. Bunsen-Ges. Phys. Chem.* **1992**, *96*, 1486.
(7) Sander, M. U.; Luther, K.; Troe, J. *J. Phys. Chem.* **1993**, *97*, 11489.
(8) Reuther, A.; Laubereau, A.; Nikogosyan, D. N. *J. Phys. Chem.* **1996**, *100*, 16794.
(9) Crowell, R. A.; Bartels, D. M. *J. Phys. Chem.* **1996**, *100*, 17940.
(10) Long, F. H.; Lu, H.; Eisenthal, K. B. *Phys. Rev. Lett.* **1990**, *64*, 1469.
(11) Shi, X.; Long, F. H.; Lu, H.; Eisenthal, K. B. *J. Phys. Chem.* **1996**, *100*, 11903.
(12) Shi, X.; Long, F. H.; Lu, H.; Eisenthal, K. B. *J. Phys. Chem.* **1995**, *99*, 6917.
(13) Migus, A.; Gauduel, Y.; Martin, J. L.; Antonetti, A. *Phys. Rev. Lett.* **1987**, *58*, 1559.
(14) Gauduel, Y.; Pommeret, S.; Migus, A.; Antonetti, A. *J. Phys. Chem.* **1991**, *95*, 533.
(15) Mcgowen, J. L.; Ajo, H. M.; Zhang, J. Z.; Schwartz, B. J. *Chem. Phys. Lett.* **1994**, *231*, 504.
(16) Pépin, C.; Houde, D.; Remita, H.; Goulet, T.; Jay-Gerin, J.-P. *Phys. Rev. Lett.* **1992**, *69*, 3389.
(17) Pépin, C.; Goulet, T.; Houde, D.; Jay-Gerin, J. P. *J. Phys. Chem. A* **1997**, *101*, 4351.
(18) Pépin, C.; Goulet, T.; Houde, D.; Jay-Gerin, J.-P. *J. Phys. Chem.* **1994**, *98*, 7009.

(19) Turi, L.; Holpar, P.; Keszei, E.; Pépin, C.; Houde, D. *J. Phys. Chem. A* **1997**, *101*, 5469.
(20) Schwartz, B. J.; Rossky, P. J. *J. Chem. Phys.* **1994**, *101*, 6902.
(21) Schwartz, B. J.; Rossky, P. J. *J. Chem. Phys.* **1994**, *101*, 6917.
(22) Schwartz, B. J.; Rossky, P. J. *J. Chem. Phys.* **1996**, *105*, 6997.
(23) Schwartz, B. J.; Bittner, E. R.; Prezhdo, O. V.; Rossky, P. J. *J. Chem. Phys.* **1996**, *104*, 5942.
(24) Prezhdo, O. V.; Rossky, P. J. *J. Phys. Chem.* **1996**, *100*, 17094.
(25) Bratos, S.; Leicknam, J.-C. *Chem. Phys. Lett.* **1996**, *261*, 117.
(26) Bratos, S.; Leicknam, J.-C.; Borgis, D.; Staib, A. *Phys. Rev. E* **1997**, *55*, 7217.
(27) Borgis, D.; Bratos, S. *J. Mol. Struct.* **1997**, *436*−*437*, 537.
(28) Borgis, D.; Staib, A. *Chem. Phys. Lett.* **1994**, *230*, 405.
(29) Staib, A.; Borgis, D. *J. Chem. Phys.* **1995**, *103*, 2642.
(30) Barnett, R. B.; Landman, U.; Nitzan, A. *J. Chem. Phys.* **1989**, *90*, 4413.
(31) Neria, E.; Nitzan, A. *Chem. Phys.* **1994**, *183*, 351.
(32) Graf, P.; Nitzan, A.; Diercksen, G. H. F. *J. Phys. Chem.* **1996**, *100*, 18916.
(33) Schnitker, J.; Motakabbir, K.; Rossky, P. J.; Friesner, R. *Phys. Rev. Lett.* **1988**, *60*, 456.
(34) Spirk, M.; Impey, R. W.; Klein, M. L. *J. Stat. Phys.* **1986**, *43*, 967.
(35) Wallqvist, A.; Martyna, G.; Berne, B. J. *J. Phys. Chem.* **1988**, *92*, 1721.
(36) Romero, C.; Jonah, C. D. *J. Chem. Phys.* **1989**, *90*, 1877.
(37) Fleming, G. R.; Cho, M. *Annu. Rev. Phys. Chem.* **1996**, *47*, 109.
(38) Maroncelli, M. *J. Mol. Liq.* **1993**, *57*, 1.
(39) Bagchi, B.; Chandra, A. *J. Chem. Phys.* **1992**, *97*, 5126.
(40) Roy, S.; Bagchi, B. *J. Chem. Phys.* **1993**, *99*, 9938.
(41) Nandi, N.; Roy, S.; Bagchi, B. *J. Chem. Phys.* **1995**, *102*, 1390.
(42) Raineri, F. O.; Resat, H.; Perng, B.-C.; Hirata, F.; Friedman, H. L. *J. Chem. Phys.* **1994**, *100*, 1477.
(43) Maroncelli, M.; Kumar, V. P.; Papazyan, A. *J. Phys. Chem.* **1993**, *97*, 13.
(44) Maroncelli, M.; Fleming, G. R. *J. Chem. Phys.* **1988**, *89*, 5044.
(45) Karim, O. A.; Haymet, A. D. J.; Banet, M. J.; Simon, J. D. *J. Phys. Chem.* **1988**, *92*, 3391.
(46) Levy, R. M.; Kitchen, D. B.; Blair, J. T.; Krogh-Jespersen, K. *J. Phys. Chem.* **1990**, *94*, 4470.
(47) Huang, J. K.; King, G.; Creighton, S.; Warshel, A. *J. Am. Chem. Soc.* **1988**, *110*, 5297.
(48) Bader, J. S.; Chandler, D. *Chem. Phys. Lett.* **1989**, *157*, 501.
(49) Rossky, P. J.; Schnitker, J. *J. Phys. Chem.* **1988**, *92*, 4277.
(50) Stratt, R. M.; Cho, M. H. *J. Chem. Phys.* **1994**, *99*, 6700.
(51) Cho, M.; Fleming, G. R.; Saito, S.; Ohmine, I.; Stratt, R. M. *J. Chem. Phys.* **1994**, *100*, 6672.
(52) Ladanyi, B. M.; Stratt, R. M. *J. Phys. Chem.* **1995**, *99*, 2502.
(53) Muiño, P.; Callis, P. R. *J. Chem. Phys.* **1994**, *100*, 4093.
(54) Jimenez, R.; Fleming, G. R.; Kumar, P. V.; Maroncelli, M. *Nature* **1994**, *369*, 471.
(55) Rosenthal, S. J.; Xie, X.; Du, M.; Fleming, G. R. *J. Chem. Phys.* **1991**, *95*, 4715.
(56) Rosenthal, S. J.; Jimenez, R.; Fleming, G. R.; Kumar, P. V.; Maroncelli, M. *J. Mol. Liq.* **1994**, *60*, 25.
(57) Horng, M. L.; Gardecki, J. A.; Papazyan, A.; Maroncelli, M. *J. Phys. Chem.* **1995**, *99*, 17311.
(58) Bingemann, D.; Ernsting, N. P. *J. Chem. Phys.* **1995**, *102*, 2691.
(59) Joo, T.; Jia, Y.; Yu, J.-Y.; Lang, M. J.; Fleming, G. R. *J. Chem. Phys.* **1996**, *104*, 6089.
(60) Cho, M.; Yu, J.-Y.; Joo, T.; Nagasawa, Y.; Passino, S.; Fleming, G. R. *J. Phys. Chem.* **1996**, *100*, 11944.
(61) Castner, E. W.; Chang, Y. J.; Chu, Y. C.; Walrafen, G. E. *J. Chem. Phys.* **1995**, *102*, 653.
(62) Palese, S.; Mukamel, S.; Miller, R. J. D.; Lotshaw, W. T. *J. Phys. Chem.* **1996**, *100*, 10380.
(63) Asaki, M. T.; Huang, C. P.; Garvey, D.; Zhou, J.; Murnane, M. M.; Kapteyn, H. C. *Opt. Lett.* **1993**, *18*, 977.
(64) Backus, S.; Peatross, J.; Huang, C. P.; Murnane, M. M.; Kapteyn, H. C. *Opt. Lett.* **1995**, *20*, 2000.
(65) Kliner, D. A. V.; Alfano, J. C.; Barbara, P. F. *J. Chem. Phys.* **1993**, *98*, 5375.
(66) Kummrow, A.; Emde, M. F.; Baltuska, A.; Pshenichnikov, M. S.; Wiersma, D. A. *J. Phys. Chem. A* **1998**, *102*, 4172.
(67) Jou, F.-Y.; Freeman, G. R. *J. Phys. Chem.* **1979**, *83*, 2385.
(68) Rips, I. *Chem. Phys. Lett.* **1995**, *245*, 79.
(69) Blandamer, M. J.; Fox, M. F. *Chem. Rev.* **1970**, *70*, 59.
(70) Long, F. H.; Lu, H.; Shi, X.; Eisenthal, K. B. *Chem. Phys. Lett.* **1990**, *169*, 165.
(71) Long, F. H.; Shi, X.; Lu, H.; Eisenthal, K. B. *J. Phys. Chem.* **1994**, *98*, 7252.
(72) Gauduel, Y.; Gelabert, H.; Ashokkumar, M. *J. Mol. Liq.* **1995**, *64*, 57.
(73) Gauduel, Y.; Gelabert, H.; Ashokkumar, M. *Chem. Phys.* **1995**, *197*, 167.
(74) Sheu, W.-S.; Rossky, P. J. *J. Am. Chem. Soc.* **1993**, *115*, 7729.
(75) Sheu, W.-S.; Rossky, P. J. *Chem. Phys. Lett.* **1993**, *213*, 233.
(76) Sheu, W.-S.; Rossky, P. J. *J. Phys. Chem.* **1996**, *100*, 1295.
(77) Staib, A.; D, B. *J. Chem. Phys.* **1996**, *104*, 9027.
(78) Jonah, C. D.; Bartels, D. M.; Chernovitz, A. C. *Radiat. Phys. Chem.* **1989**, *34*, 145.